AIAA Guidance, Navigation and Control Conference and Exhibit
20 - 23 August 2007, Hilton Head, South Carolina

AIAA 2007-6324

Minimum-Power Robotic Maneuvering Using Control-Moment Gyroscopes

Michele D. Carpenter* and Mason A. Peck†
Cornell University, Ithaca, New York, 14853

Control-moment gyroscopes (CMGs) are power-efficient actuators that typically provide high torques to large spacecraft. In this study, we propose the use of CMGs in actuating a space robotic arm, whose tasks include manipulating a payload. This paper derives the full nonlinear equations of motion for a three degree-of-freedom system with a mass-center offset and incorporates a closed-loop control design. Under a controlled motion, we demonstrate that a CMG-driven robotic arm can manipulate a payload with minimal changes to the system energy. By investigating how a payload affects the dynamics for single-body and multi-body systems, we find that the equations of motion and expressions for power are simpler when the individual bodies are moved sequentially. However, by comparing both sequential and simultaneous body motions for randomly chosen maneuvers, we show that less energy is expended on average when the bodies are controlled simultaneously.

I. Introduction

PREVIOUS work has established that control-moment gyroscopes (CMGs) are a power-efficient means to actuate a robotic arm in space.[1–3] A CMG is a torque actuator primarily used for the attitude control of large spacecraft. It consists of a constant-speed rotor and a gimbal that changes the direction of the rotor's angular-momentum vector. Since this change in angular momentum generates a gyroscopic torque orthogonal to the gimbal axis, it is purely a constraint torque that does no work. If the CMG were fixed and lossless and if the gimbaled inertia were zero, the CMG would require no input power.

Steering a gimbaled payload independently of the spacecraft bus can be accomplished in many ways, including the obvious application of torque to each joint by a motor. However, many approaches produce a reaction torque on the spacecraft that may cause undesirable dynamic behavior of the rotating bodies that comprise the gimbaled payload. This effect may also degrade the performance of an attitude control system that must maintain precise pointing of the spacecraft. This study investigates an approach that is largely reactionless since the robotic arm is actuated by internal momentum exchange. A reactionless robotic segment might use a simple internal reaction wheel, a device whose rotor accelerates about an axis fixed to the body on which it is mounted. Such a segment can exhibit constant angular momentum during actuation and therefore react no torque onto the spacecraft bus. However, reaction wheels provide high torque only at the expense of high electromechanical power,

$$P = \boldsymbol{\tau} \cdot \boldsymbol{\omega}, \tag{1}$$

where P is the shaft power imparted by the wheel and $\boldsymbol{\tau}$ represents the vector torque that is applied by the reaction wheel when the rotor speed $\boldsymbol{\omega}$ is changed. In practice, CMGs offer orders of magnitude higher torque for the power of an equivalent reaction wheel. Our previous work addressed the high-agility and low-power features of a three-link robotic arm actuated by CMGs when compared to reaction wheels.[1] This work assumed spherical arm segments with the system mass center on the axis of the inboard joint such that reaction forces and torques are absent from the equations of motion. When prescribing the CMG gimbal kinematics in an open loop, this system was able to execute a maneuver with less than one percent of the

*Graduate Student, Department of Theoretical and Applied Mechanics, 236 Thurston Hall, AIAA Student Member.
†Assistant Professor, Department of Mechanical and Aerospace Engineering, 212 Upson Hall, AIAA Member.

power required by an equivalent system driven by reaction wheels.

This study evaluates the use of CMGs in a spacecraft-mounted robotic arm, one of whose tasks involves manipulating a payload. We define the system kinematics, derive the equations of motion, and use those equations to demonstrate a feedback control strategy for moving a payload in an arbitrary pick-and-place maneuver. Since CMGs produce torques by redistributing momentum within the system during a maneuver, motion is achieved with minimal changes in system energy. If such a concept can be demonstrated, it may be used as one of many starting points for new developments in space robotics.

II. System Description and Kinematics

To perform a general pick-and-place maneuver, the system must be able to operate in three degrees of freedom. We propose a three-segment robotic arm interconnected with single degree-of-freedom revolute joints. The joint axis of a given body is orthogonal to that of its inboard neighbor. Each body carries a single scissored pair of CMGs.[1–5] A scissored pair, shown in Fig. 1, consists of two identical, single-gimbal CMGs that share a gimbal axis. The CMGs rotate with equal-magnitude gimbal angles in opposite directions. In this configuration, the rotor angular-momentum vectors $\mathbf{h}_1$ and $\mathbf{h}_2$ rotate in a plane orthogonal to the gimbal axis such that their vector sum always lies along the joint axis. The net torque imparted to the body by each CMG is also parallel to the joint axis and is nonsingular only at saturation, when both CMG rotor angular-momentum vectors are parallel.

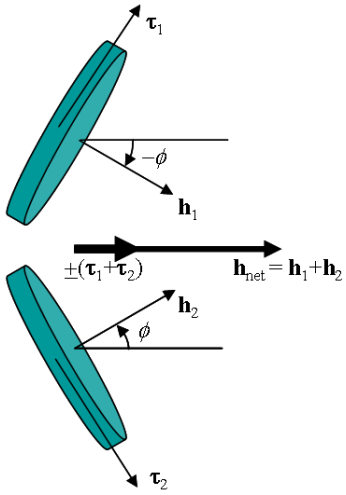

Figure 1. Top-view schematic of a CMG scissored pair.

Figure 2 illustrates a three-body concept for the payload problem that can be extended to an arbitrary number of bodies.

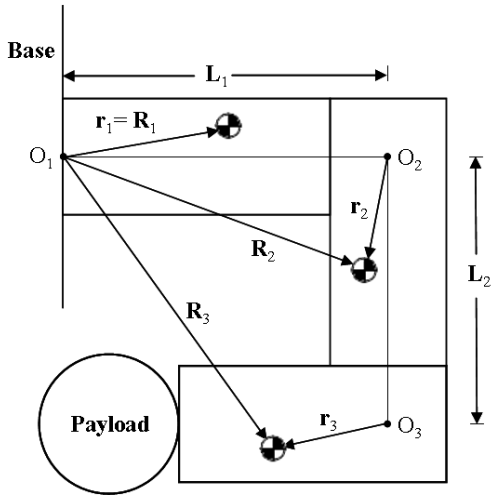

Figure 2. System concept for the payload problem.

Our previous work has shown that the total angular momentum of N linked bodies with CMG scissored pairs is given by

$$\mathbf{H} = \sum_{i=1}^{N} \mathbf{H}_i = \sum_{i=1}^{N} \mathbf{I}_{i\mathrm{C}} \cdot \boldsymbol{\omega}^{i/0} + \mathbf{R}_i \times m_{i\mathrm{C}} \mathbf{V}_i + 2\mathrm{h}_i \cos\phi_i \hat{\mathbf{e}}_{i1}, \tag{2}$$

where $\mathbf{H}_i$ is the angular momentum of body i about the fixed point O_1 at the intersection of the innermost body's joint axis with the stationary base. $\mathbf{I}_{i\mathrm{C}}$ is the composite inertia dyadic about the mass center for the ith arm segment-CMG scissored pair combination with total mass, $m_{i\mathrm{C}}$. ϕ_1 is the angular distance of $\mathbf{h}_1$ and $\mathbf{h}_2$ from the joint axis, and $\hat{\mathbf{e}}_{ij}$ represents the basis vector along the j direction in the coordinate system fixed to body i. Reference frames are numbered, with 0 corresponding to the inertial frame and $1, 2, \ldots, N$ corresponding to the frames fixed to each arm segment from innermost to outermost. $\boldsymbol{\omega}^{i/j}$ is the angular velocity of frame i relative to frame j, while $\mathbf{R}_i$ and $\mathbf{V}_i$ are the position and velocity vectors for the mass center of body i measured from O_1.

The total torque on this N-body system is the derivative of the system angular momentum in an inertial frame,

$$\begin{aligned} \frac{{}^0d}{dt}\mathbf{H} = \sum_{i=1}^{N} \frac{{}^0d}{dt}\mathbf{H}_i = \sum_{i=1}^{N} \mathbf{I}_{i\mathrm{C}} \cdot \frac{{}^id}{dt}\boldsymbol{\omega}^{i/0} + \boldsymbol{\omega}^{i/0} \times \mathbf{I}_{i\mathrm{C}} \cdot \boldsymbol{\omega}^{i/0} + \mathbf{R}_i \times m_{i\mathrm{C}} \mathbf{A}_i \\ +2\mathrm{h}_i \left(-\dot{\phi}_i \sin\phi_i \hat{\mathbf{e}}_{i1} + \boldsymbol{\omega}^{i/0} \times \cos\phi_i \hat{\mathbf{e}}_{i1} \right), \end{aligned} \tag{3}$$

where $\mathbf{A}_i$ is the inertial acceleration vector for the mass center of body i. Equation (3) provides a basis for extracting the equations of motion using Kane's method.[6,7] With the reference configuration shown in Fig. 3 and described in Ref. 1, we find that the general transformation from the body j-fixed coordinate system to the body i-fixed coordinate system is

$${}^iQ^j = \prod_{k=i}^{j-1} L \cdot \left\{ \cos\theta_{k+1} \mathbf{1} + (1 - \cos\theta_{k+1}) \begin{bmatrix} 1 & 0 & 0 \\ 0 & 0 & 0 \\ 0 & 0 & 0 \end{bmatrix} + \sin\theta_{k+1} \begin{bmatrix} 0 & 0 & 0 \\ 0 & 0 & -1 \\ 0 & 1 & 0 \end{bmatrix} \right\}, \tag{4}$$

where $\mathbf{1}$ is the identity matrix in $\mathbb{R}^{3\times3}$ and θ_i is the angle of body i relative to body $i-1$. Since adjacent coordinate systems are not aligned in this reference configuration, a linear transformation L is performed on the rotation matrix.

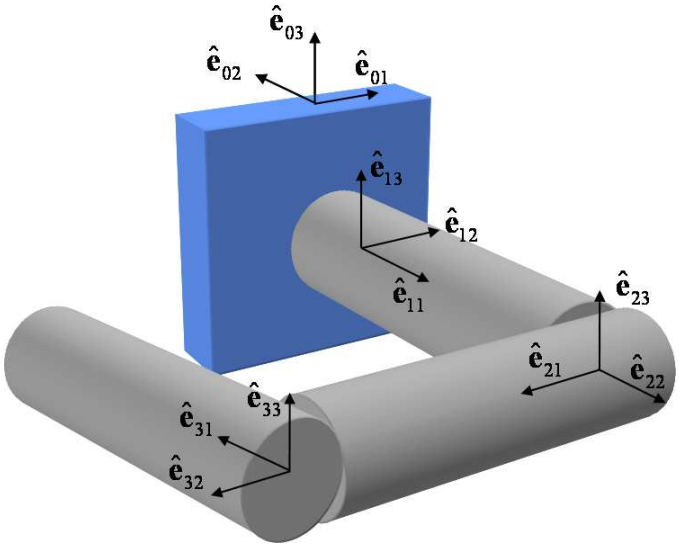

Figure 3. Clockwise-spiral reference configuration for a multi-body system.

A representation of the end-effector kinematics provides the basis for controlling its motion along an arbitrary path. Path planning refers to the problem of specifying a sequence of arm segment positions and orientations that move the end effector between two points. Motion planning takes into account both the system dynamics and kinematics. We define the payload trajectory and convert it into a set of desired joint angles by applying the inverse kinematics. However, an analytical representation of these inverse kinematics may not be available, even for three degree-of-freedom manipulators.[8] Instead of dealing with the increments of external and joint coordinates, one can exploit the relationship between the velocities:

$$\begin{bmatrix} \dot{x}_e \\ \dot{y}_e \\ \dot{z}_e \end{bmatrix} = J \cdot \begin{bmatrix} \dot{\theta}_1 \\ \dot{\theta}_2 \\ \vdots \\ \dot{\theta}_N \end{bmatrix}. \tag{5}$$

In order to find this relationship between the joint rates and the velocities in external coordinates, we first define the position of the end effector using a common approach for such systems. If the end effector is located at the mass center of the combined outer body and payload, then according to Fig. 2, its position, velocity, and acceleration vectors relative to the base frame are

$$\mathbf{R}_e = \mathbf{R}_i = \sum_{j=1}^{i-1} \mathbf{L}_j + \mathbf{r}_i \tag{6}$$

$$\mathbf{V}_e = \mathbf{V}_i = \sum_{j=1}^{i-1} \left(\boldsymbol{\omega}^{j/0} \times \mathbf{L}_j \right) + \boldsymbol{\omega}^{i/0} \times \mathbf{r}_i \tag{7}$$

$$\mathbf{A}_e = \mathbf{A}_i = \sum_{j=1}^{i-1} \left(\frac{^j d}{dt} \boldsymbol{\omega}^{j/0} \times \mathbf{L}_j + \boldsymbol{\omega}^{j/0} \times (\boldsymbol{\omega}^{j/0} \times \mathbf{L}_j) \right) + \frac{^i d}{dt} \boldsymbol{\omega}^{i/0} \times \mathbf{r}_i + \boldsymbol{\omega}^{i/0} \times (\boldsymbol{\omega}^{i/0} \times \mathbf{L}_i). \tag{8}$$

$\mathbf{L}_i$ represents the constant-length position vector from the origin of the body $i-1$ frame to the origin of the body i frame, and $\mathbf{r}_i$ is a constant-length position vector of the body i mass center relative to the body i frame.

Choosing the generalized coordinates to be the relative body angles $q_j = \theta_j$, we differentiate Eq. (7) with respect to each of the generalized velocities, $\dot{q}_j = \dot{\theta}_j$, to find the Jacobian relating the joint rates and the end-effector velocity in external coordinates.

$$\frac{\partial \mathbf{V}_e}{\partial \dot{q}_j} = \begin{cases} \hat{\mathbf{e}}_{j1} \times \left(\sum_{k=1}^{i-1} \mathbf{L}_k + \mathbf{r}_i \right) & i > j \\ \hat{\mathbf{e}}_{j1} \times \mathbf{r}_i & i = j \\ 0 & i < j \end{cases} \tag{9}$$

This Jacobian is used to compute the joint rate error for use by a controller that keeps the end effector on a specified path. The following evaluation of the performance of this system involves only the control of joint motions and does not consider the resulting end-effector motions. Nevertheless, this kinematic description provides sufficient generality for other analyses.

III. System Dynamics

To describe the dynamics of a general N-link system, we first consider a very simple case without a payload, where the system consists of spherical bodies with each mass center on the joint axis. A full derivation of the equations of motion for this system is provided in Ref. 1. To summarize, we know that since the body mass centers do not translate during payload motions, there are no inertial forces on the system acting between the innermost body and the stationary base. The only generalized active torque on the system is the contact torque due to friction between the innermost body and the base. However, in this ideal case, we assume a frictionless contact. There are also constraint torques applied between each body, but they do not contribute to the generalized active torques and therefore do not appear in the equations of motion. Finally, the system inertia dyadic is constant in an inertial frame during body rotations such that there are no external torques. With purely internal torques and a stationary system mass center, Kane's method yields the general equations of motion:

$$\sum_{i=1}^{N} \frac{{}^0 d}{dt} \mathbf{H}_i \cdot \frac{\partial \boldsymbol{\omega}_i}{\partial \dot{q}_j} = 0. \tag{10}$$

In Eq. (10), $\boldsymbol{\omega}_i$ is the angular velocity of body i relative to an inertial frame. Each generalized coordinate is the angular position of a body relative to its neighboring inboard body, $q_j = \theta_j$, and the generalized velocities are the time derivatives of the generalized coordinates, $\dot{q}_j = \dot{\theta}_j$. If N is the total number of masses and M is the number of degrees of freedom, then $i = 1, \ldots, N$ and $j = 1, \ldots, M$.

Once the payload is acquired, the problem becomes more complicated. It is assumed that the payload and outboard arm segment form a single augmented outboard body. The augmented outboard body differs from the inboard bodies in its mass and in the fact that the mass center is offset from the axis of rotation. In Fig. 4, O_3 is the origin of the body 3-fixed coordinate system, $\mathbf{r}_p$ is the position vector from O_3 to the payload center of mass, $\mathbf{r}_3$ is the position vector from O_3 to the body 3 center of mass, and $\mathbf{r}_{3p}$ is the position vector from O_3 to the combined center of mass.

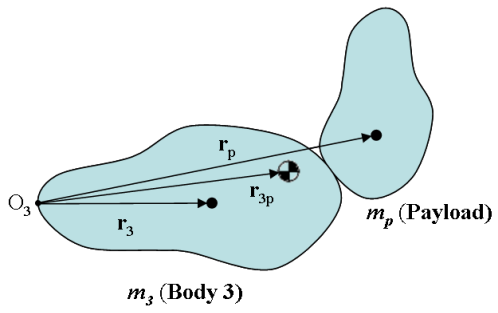

Figure 4. Schematic of outboard arm segment with attached payload.

If $\mathbf{a} = \mathbf{r}_{3p} - \mathbf{r}_3$ and $\mathbf{b} = \mathbf{r}_p - \mathbf{r}_{3p}$, the inertia dyadic $\mathbf{I}_{3p}$ of the augmented outer body about its mass center is determined by the parallel axis theorem[9]

$$\mathbf{I}_{3\text{tot}} = \mathbf{I}_3 + \mathbf{I}_p - m_3(a^2\mathbf{1} - \mathbf{aa}) - m_p(b^2\mathbf{1} - \mathbf{bb}), \tag{11}$$

where $\mathbf{I}_3$ is the central inertia dyadic of the outer arm segment without the CMGs, $\mathbf{I}_p$ is the central inertia dyadic of the payload, and a and b are the magnitudes of $\mathbf{a}$ and $\mathbf{b}$, respectively. Considering this calculation, an added payload causes the appearance of products of inertia in the inertia matrix of the outer body, the addition of mass, and a change in the location of the outer body's mass center. Further, the mass-center offset implies that there is an inertial force due to its acceleration during a maneuver. We use Kane's method, as in the previous example without a payload, to find the equations of motion for this system. In this more general case with a mass offset due to an added payload, the equations of motion are

$$\sum_{i=1}^{N}\left(m_{i\mathrm{C}}\mathbf{A}_i - \mathbf{F}_i^a\right)\cdot\frac{\partial\mathbf{V}_i}{\partial\dot{q}_j} + \left(\frac{{}^0d}{dt}\mathbf{H}_i - \mathbf{M}_i^a\right)\cdot\frac{\partial\boldsymbol{\omega}_i}{\partial\dot{q}_j} = 0, \tag{12}$$

where $\mathbf{F}_i^a$ is the total active force that does work on body i and $\mathbf{M}_i^a$ is the total active moment that does work on body i.

Finally, in order to examine the power consumption of an N-body system, we first derive its total energy, which is entirely kinetic:

$$\begin{aligned} 2\mathrm{E}_{\text{tot}} = \sum_{i=1}^{N} 2\mathrm{E}_i \quad &= \quad \sum_{i=1}^{N} \boldsymbol{\omega}^{i/0}\cdot\mathbf{I}_i\cdot\boldsymbol{\omega}^{i/0} + \boldsymbol{\omega}^{\mathrm{G}_{i1}/0}\cdot\mathbf{I}_{\mathrm{G}_{i1}}\cdot\boldsymbol{\omega}^{\mathrm{G}_{i1}/0} + \boldsymbol{\omega}^{\mathrm{G}_{i2}/0}\cdot\mathbf{I}_{\mathrm{G}_{i2}}\cdot\boldsymbol{\omega}^{\mathrm{G}_{i2}/0} \\ &\quad + \boldsymbol{\omega}^{\mathrm{R}_{i1}/0}\cdot\mathbf{I}_{\mathrm{R}_{i1}}\cdot\boldsymbol{\omega}^{\mathrm{R}_{i1}/0} + \boldsymbol{\omega}^{\mathrm{R}_{i2}/0}\cdot\mathbf{I}_{\mathrm{R}_{i2}}\cdot\boldsymbol{\omega}^{\mathrm{R}_{i2}/0}. \end{aligned} \tag{13}$$

In Eq. (13), $\mathbf{I}_i$ is the central inertia dyadic of the ith arm segment without the CMGs. $\mathbf{I}_{\mathrm{G}_{ij}}$ is the central inertia dyadic of the jth gimbal on body i and $\mathbf{I}_{\mathrm{R}_{ij}}$ is the central inertia dyadic of the jth CMG rotor on body i. In addition, G_{ij} and R_{ij} also represent the jth gimbal-fixed frame on body i and the jth rotor-fixed frame on body i, respectively.

The time derivative of Eq. (13) yields the total power of the system:

$$\begin{aligned} \mathrm{P}_{\text{tot}} = \sum_{i=1}^{N} \dot{\mathrm{E}}_i \quad &= \quad \sum_{i=1}^{N} \frac{{}^i d}{dt}\boldsymbol{\omega}^{i/0}\cdot\mathbf{I}_i\cdot\boldsymbol{\omega}^{i/0} + \frac{{}^{\mathrm{G}_{i1}}d}{dt}\boldsymbol{\omega}^{\mathrm{G}_{i1}/0}\cdot\mathbf{I}_{\mathrm{G}_{i1}}\cdot\boldsymbol{\omega}^{\mathrm{G}_{i1}/0} + \frac{{}^{\mathrm{G}_{i2}}d}{dt}\boldsymbol{\omega}^{\mathrm{G}_{i2}/0}\cdot\mathbf{I}_{\mathrm{G}_{i2}}\cdot\boldsymbol{\omega}^{\mathrm{G}_{i2}/0} \\ &\quad + \frac{{}^{\mathrm{R}_{i1}}d}{dt}\boldsymbol{\omega}^{\mathrm{R}_{i1}/0}\cdot\mathbf{I}_{\mathrm{R}_{i1}}\cdot\boldsymbol{\omega}^{\mathrm{R}_{i1}/0} + \frac{{}^{\mathrm{R}_{i2}}d}{dt}\boldsymbol{\omega}^{\mathrm{R}_{i2}/0}\cdot\mathbf{I}_{\mathrm{R}_{i2}}\cdot\boldsymbol{\omega}^{\mathrm{R}_{i2}/0}. \end{aligned} \tag{14}$$

However, as Ref. 1 describes, negative values of power indicate energy extracted from the motion of the connected components. This energy-recovery process cannot be perfect, and in practice it is likely inefficient. Energy losses represent friction in the motors and $\mathrm{I}^2\mathrm{R}$ dissipation due to heat created by current and resistance. In the likely case where the robotic arm is not designed to regeneratively recover this energy through generators and batteries, the system's power consumption is bounded by the sum of the absolute values of power computed for each system component.

A general description of the robot's dynamics provides the means to understand a payload's effect on power consumption. We do so by first considering a few simple cases, beginning with the single-body system shown in Fig. 5.

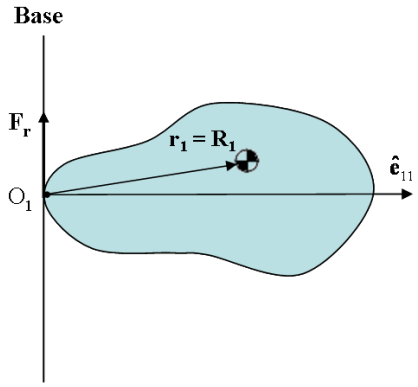

Figure 5. Single-body system with mass-center offset from joint axis.

This system consists of a single arm segment with a scissored pair of CMGs, whose combined mass center is offset from the joint axis. This offset causes the mass center to accelerate relative to an inertial frame as the body rotates. We can therefore use Eq. (12), with $N = 1$, to describe its dynamics. However, since the inertial force due to this acceleration is reacted onto the stationary base, it vanishes from the equation of motion as a workless constraint force. Since there are no active forces and torques on the system, Eq. (12) reduces to

$$\frac{{}^0d}{dt}\mathbf{H}_1 \cdot \frac{\partial \boldsymbol{\omega}_1}{\partial \dot{q}_1} = 0. \tag{15}$$

We calculate the torque on this system using Eq. (3) with $N = 1$

$$\frac{{}^0d}{dt}\mathbf{H}_1 = \mathbf{I}_{1\mathrm{C}} \cdot \frac{{}^1d}{dt}\boldsymbol{\omega}^{1/0} + \boldsymbol{\omega}^{1/0} \times \mathbf{I}_{1\mathrm{C}} \cdot \boldsymbol{\omega}^{1/0} + \mathbf{R}_1 \times m_{1\mathrm{C}}\mathbf{A}_1 - 2\mathrm{h}_1\dot{\phi}_1 \sin\phi_1 \hat{\mathbf{e}}_{11}, \tag{16}$$

and find that when expressed in body 1 coordinates, this torque is

$$\frac{{}^0d}{dt}\mathbf{H}_1 = \begin{bmatrix} \left(\mathrm{I}_{11} + m_{1\mathrm{C}}\mathrm{R}_{1,2}^2 + m_{1\mathrm{C}}\mathrm{R}_{1,3}^2\right)\ddot{\theta}_1 - 2\mathrm{h}_1\dot{\phi}_1 \sin\phi_1 \\ \left(\mathrm{I}_{12} - m_{1\mathrm{C}}\mathrm{R}_{1,1}\mathrm{R}_{1,2}\right)\ddot{\theta}_1 - \mathrm{I}_{13}\dot{\theta}_1^2 \\ \left(\mathrm{I}_{13} - m_{1\mathrm{C}}\mathrm{R}_{1,1}\mathrm{R}_{1,3}\right)\ddot{\theta}_1 + \mathrm{I}_{12}\dot{\theta}_1^2 \end{bmatrix}, \tag{17}$$

where $\mathrm{R}_{1,i}$ are the components of $\mathbf{R}_1$ and I_{ij} are the elements of the inertia matrix $\mathbf{I}_{1\mathrm{C}}$. The projection of Eq. (17) onto the partial angular velocity vector, or the basis vector along the joint axis, remains the same with the exception of additional $m\mathrm{R}^2$ terms. Therefore, in this single-body system, a mass-center offset affects only inertia in the equation of motion. It is also interesting to note that while the total angular momentum changes because of the reacted constraint force at the base, the CMGs only act in the direction along which angular momentum is conserved.

We repeat this analysis for a two-body system assuming a spherical inboard body with the mass center on the joint axis and an outboard body with an arbitrary mass distribution. Part (a) of Fig. 6 is a sketch of such a configuration.

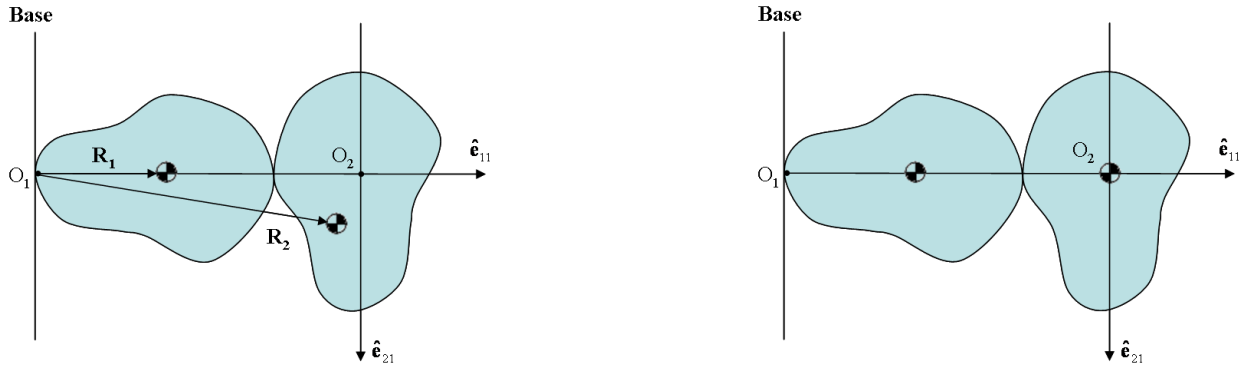

(a) With CM offset.

(b) Without CM offset.

Figure 6. Two-body system.

First, we compute the torque on body 1 with Eq. (16) and then find the torque on body 2:

$$\frac{{}^0d}{dt}\mathbf{H}_2 = \mathbf{I}_{2\mathrm{C}} \cdot \frac{{}^2d}{dt}\boldsymbol{\omega}^{2/0} + \boldsymbol{\omega}^{2/0} \times \mathbf{I}_{2\mathrm{C}} \cdot \boldsymbol{\omega}^{2/0} + \mathbf{R}_2 \times m_{2\mathrm{C}}\mathbf{A}_2 + 2\mathrm{h}_2 \left[-\dot{\phi}_2 \sin\phi_2 \hat{\mathbf{e}}_{21} + \boldsymbol{\omega}^{2/0} \cos\phi_2 \times \hat{\mathbf{e}}_{21}\right]. \quad (18)$$

To further analyze the system, we define the kinematics. Since the position vector of the inner body's mass center relative to an inertial frame has constant length and is coincident with the joint axis, the inner body's mass center is stationary. However, the position and inertial velocity vectors of the outer body's mass center are given by Eqs. (6)-(7) with $i = 2$. We compute the partial velocities and partial angular velocities and use Kane's method in Eq. (12) with $N = 2$ to determine the equations of motion. The inertial force on the outer body expressed in body 2 coordinates is

$$m_{2\mathrm{C}} \cdot {}^2\mathrm{A}_2 = m_{2\mathrm{C}} \cdot \begin{bmatrix} \ddot{\theta}_1 \left(\mathrm{r}_{2,2}\sin\theta_2 + \mathrm{r}_{2,3}\cos\theta_2\right) + 2\dot{\theta}_1\dot{\theta}_2 \left(\mathrm{r}_{2,2}\cos\theta_2 - \mathrm{r}_{2,3}\sin\theta_2\right) - \dot{\theta}_1^2\mathrm{r}_{2,1} \\ -\ddot{\theta}_1\mathrm{r}_{2,1}\sin\theta_2 - \ddot{\theta}_2\mathrm{r}_{2,3} - \dot{\theta}_1^2\left(\mathrm{r}_{2,2}\sin^2\theta_2 + \mathrm{r}_{2,3}\sin\theta_2\cos\theta_2\right) - \dot{\theta}_2^2\mathrm{r}_{2,2} \\ -\ddot{\theta}_1\mathrm{r}_{2,1}\cos\theta_2 + \ddot{\theta}_2\mathrm{r}_{2,2} - \dot{\theta}_1^2\left(\mathrm{r}_{2,3}\cos^2\theta_2 + \mathrm{r}_{2,2}\sin\theta_2\cos\theta_2\right) - \dot{\theta}_2^2\mathrm{r}_{2,3} \end{bmatrix}, \quad (19)$$

where $\mathrm{r}_{2,i}$ are the components of $\mathbf{r}_2$. With the additional inertial torques and forces in Eqs. (18) and (19), we observe that the body motions are coupled. We conclude that in general, a mass-center offset for the outer body of a two-body system cannot be treated as an inertia-only effect. This result motivates possible mass balancing such that the mass center lies on the joint axis of the inner body where it does not accelerate, as illustrated in part (b) of Fig. 6.

Our results for a single body attached to a stationary base demonstrate that there are no added forces or torques to the body's equation of motion due to a mass-center offset, which often occurs with the addition of a payload. For a two-body system, additional forces and torques are inevitable if the mass center of the outer body is off the joint axis. In an attempt to avoid complicated coupled dynamics and a possible increase in power usage, we construct a simulation for a three-body system in which the links are rotated sequentially.

For a three-body system whose links are moved in sequence, there are three possible stages for any maneuver. In one stage, the inner link rotates while the outer links are held fixed. In this situation, the fixed outer links are simply treated as an added payload. In another possible stage of the maneuver, the middle link rotates while the inner and outer links are held fixed. During this motion, the stationary inner link is considered a part of the base while the stationary outer link has the effects of an added payload on the middle link. In the final possible stage of the maneuver, the outer link rotates while the two inner links are held fixed. Here, the two inner links are considered a part of the stationary base. In any of these three situations, the resulting dynamics resemble the single-body system with its mass center offset from the joint axis. It may seem sensible to infer that, in addition to simplifying the dynamics, controlling the joints in a sequence of rotations is also the most power-efficient method of manipulating the payload. However, the reduction in total energy due to simultaneous motions may also be preferable. We take up this question via a numerical analysis in the next section.

IV. Control Design and Simulation

The full nonlinear equations of motion for the three-body system can be accommodated in a feedback-control design, with the nonlinear terms in the feedforward portion of the control loop. In order to use second-order system design principles, we seek the plant in the general form

$$\ddot{\Theta} + X\dot{\Phi} + F = 0, \tag{20}$$

where $\ddot{\Theta}$ is a column matrix of relative body angular accelerations and $\dot{\Phi}$ is a column matrix of gimbal rates.

With the equations of motion for a CMG-driven system, we first separate the angular accelerations from the gimbal rates

$$M\ddot{\Theta} + P\dot{\Phi} + V = 0. \tag{21}$$

Pre-multiplying by the mass matrix, M, the CMG equations of motion are in the desired form of Eq. (20), where $X = M^{-1}P$ and $F = M^{-1}V$. We derive a proportional-derivative (PD) feedback control law by seeking gimbal rates such that the CMG equations of motion resemble a general second-order system

$$\ddot{\Theta} + Z\dot{\Theta} + W\Theta = 0. \tag{22}$$

In Eq. (22), we define matrices $Z = \mathrm{diag}(2\zeta_1\omega_1, \ldots, 2\zeta_N\omega_N)$ and $W = \mathrm{diag}(\omega_1^2, \ldots, \omega_N^2)$, where Z represents generalized damping desired in the feedback law, and W represents generalized stiffness. A feedback control law for the CMG gimbal rates in terms of these desired performance parameters is then

$$\dot{\Phi} = X^{-1}\Big(Z\dot{\Theta}_\mathrm{e} + W\Theta_\mathrm{e} + F\Big), \tag{23}$$

where Θ_e and $\dot{\Theta}_\mathrm{e}$ are column matrices containing errors in angular position and velocity, respectively. A more sophisticated control architecture may offer certain performance benefits, but the virtues of this design include its ease of implementation and analysis. Our focus is not this specific architecture, but instead devising a means by which to implement motion profiles that will enable the analysis of power usage.

This system is controllable except in the case where the Jacobian, X, is singular, or when its determinant is zero. Thus, we encounter a singularity when

$$\prod_{i=1}^{N} \sin\phi_i = 0. \tag{24}$$

This relationship is satisfied when any gimbal angle, $\phi_i = n\pi$, $n \in \mathbb{Z}$. The physical interpretation of this condition in our robotic system is the gimbal angle at which any CMG stores its maximum angular momentum. In our case, this saturation point occurs when a CMG rotor angular-momentum vector is coincident with the joint axis. As the gimbal angles increase towards this saturation limit, the loop gain drops. To prevent this nonlinear effect from reducing gain (so that the performance of the linear PD control is constant for all gimbal angles), a matrix $G = \mathrm{diag}(\sin\phi_1, \ldots, \sin\phi_N)$ scales the gain matrices Z and W. With the resulting varying-gain feedback control law, we provide constant control performance. The control law then finally becomes

$$\dot{\Phi} = X^{-1}\Big(GZ\dot{\Theta}_\mathrm{e} + GW\Theta_\mathrm{e} + F\Big), \tag{25}$$

This approach does not prevent singularities, which must occur when the Jacobian is singular regardless of the performance. In fact, when a scissored pair is nearly saturated, the gimbal rate required to achieve a desired output torque can be impossibly high even if the Jacobian's determinant is finite. Gimbals can only rotate so fast in practice. For this reason, among others, a scissored pair may be best limited to a range of gimbal angles within which a certain maximum torque can be guaranteed for finite gimbal rates.

In order to explore the question of how to most efficiently manipulate this system, we construct a maneuver for the situation in which the bodies move simultaneously as well as sequentially. We implement

the control law in Eq. (25) and require that each body track a step input. The inertia dyadic $\mathbf{I}_{iC}$ for each arm segment with its CMGs (but without a payload) is identical to all the others. The two inboard bodies are taken to be spherical with their mass centers on their respective joint axes while the mass center of the outboardmost body is offset from its joint axis by the added payload. Multiple spherical bodies may be difficult to realize in practice, but their simplicity makes the results of this study clearer to interpret without sacrificing anything fundamental. A detailed evaluation of the efficiency of an arbitrary system of interest can just as easily be carried out with the equations of motion provided here. For this study, the simulation parameters are listed in Table 1. The rotor angular momentum of each CMG is based on that of an existing device, the Honeywell M50 CMG.[10] In this demonstration, ω_{n} and ζ are the same for each body. Finally, we assume that the gimbals begin in a configuration for which the net angular momentum of each scissored pair is zero. This condition is satisfied when the rotor angular-momentum vectors are π radians with respect to each other and perpendicular to the joint axis.[11] Since the gimbal angles in this simulation are measured from the joint axis, the initial gimbal angles are $\pm\frac{\pi}{2}$ radians for each scissored pair.

Table 1. Simulation Parameters.

Parameter	Value
Initial relative body angles, $\theta_i(t_0)$	(0, 0, 0) rad
Initial relative body rates, $\dot{\theta}_i(t_0)$	(0, 0, 0) rad/s
Damping ratio, ζ	0.707
Natural frequency, ω_{n}	π rad/s
CMG rotor angular momentum, h_i	50 Nms
Rotor spin speed, Ω_{R}	200 rad/s
Rotor inertia, I_{R}	0.25 kg-m^2
Gimbal inertia, I_{G}	0.125 kg-m^2
Body inertia, I_i	20 kg-m^2
Payload inertia, I_p	2 kg-m^2
Body mass, m_i	10 kg
Payload mass, m_p	2 kg
Body length, L_i	2 m
Position vector of CM, $\mathbf{r}_{3p}$	[1.25, 0, 0.25] m

Figure 7 shows the satisfactory completion of a ten-second maneuver for both the simultaneous and sequential cases with a step amplitude of 0.1 radians. Figures 8 and 9 show the energy and power for the duration of each simulation.

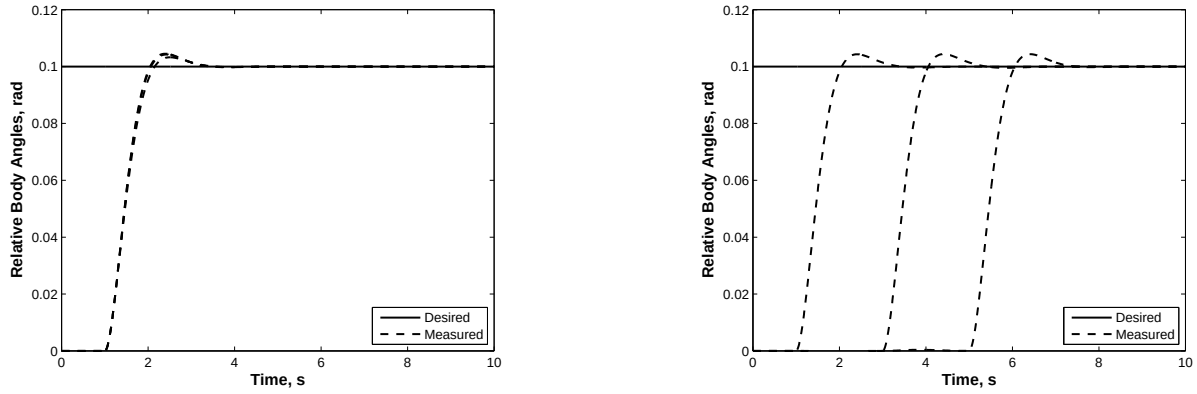

(a) Simultaneous motions.

(b) Sequential motions.

Figure 7. Relative body angles vs. time.

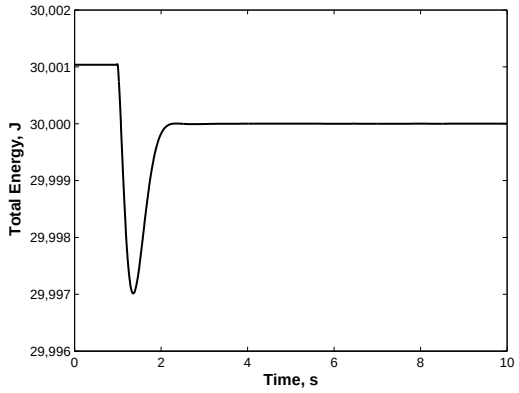

(a) Simultaneous motions.

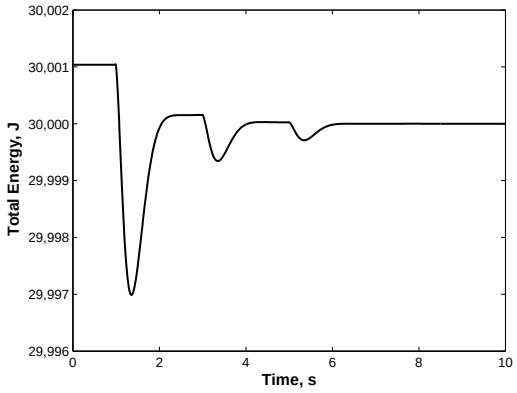

(b) Sequential motions.

Figure 8. System energy during step response.

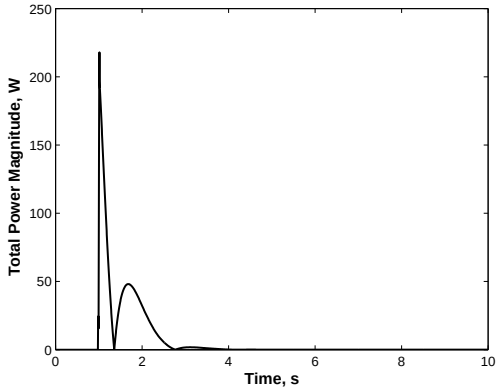

(a) Simultaneous motions.

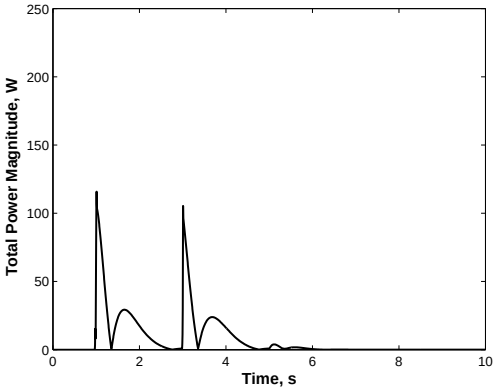

(b) Sequential motions.

Figure 9. System power during step response.

For this maneuver, the total energy expended for simultaneous motions is 68.46 J, while sequential motions cost 74.58 J. Since we initially suspected the opposite of this result, we further investigate this topic by performing a Monte Carlo simulation over the initial relative body angles, step amplitudes, and the mass-center offset of the outboard body while holding the control gains and all other simulation parameters fixed. Other than those being varied, the same parameters from Table 1 are used for this simulation. The initial body angles and step amplitudes are randomly drawn from uniform distributions over the intervals $[0, 2\pi]$ radians and $[-0.3, 0.3]$ radians, respectively. In each realization of the maneuver, the angles are different random values for each body. Varying the mass-center offset of the combined outboard body is achieved by varying the location of the payload mass center. Random draws are taken from a uniform distribution for each position component relative to the local body 3-fixed frame. The intervals for these components are: $r_{3p,1}$ = [2,3] m, $r_{3p,2}$ = [-1,1] m, and $r_{3p,3}$ = [-1,1] m. We vary these parameters to eliminate bias in the probability distribution for the energy expended. Figure 10 contains the probability distribution for both the simultaneous and sequential cases. For the simultaneous case, the mean energy expended is 100.46 J with a standard deviation of 52.55 J. For the sequential case, we find a mean of 117.57 J with a standard deviation of 57.99 J.

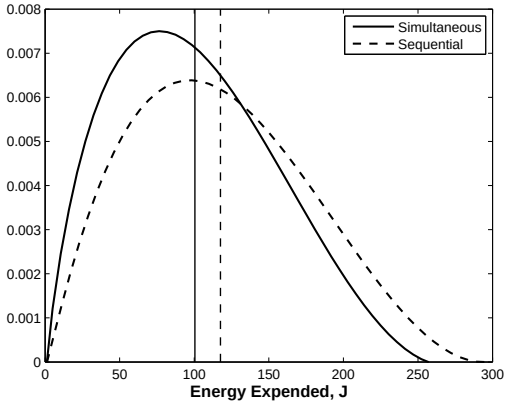

Figure 10. Probability distribution for energy expended.

These results are due to a combination of factors. In the sequential case, the controller must not only force the entire motion of the rotating body, but it must compensate for the motion reacted onto the fixed system components. During simultaneous rotations, a body can use energy from the motion of its neighbors to assist its maneuver to the desired position. To demonstrate this idea, we examine Eq. (14) for a two-body system: the simplest system that exhibits coupled motion. For sequential motions, when the outer body is rotating, Eq. (14) reduces to the single-body case with the outer body's mass properties. A rotation of the inner body also reduces Eq. (14) to the single-body case, where the mass properties of the inner body are augmented by the fixed outer body. However, for simultaneous motions, Eq. (14) is a function of the relative rates and accelerations for both bodies. In this case, some terms may be negative-valued, thus decreasing the amount of power used by a particular component. No such subtraction is possible for sequential motions because all other body rates are zero. These findings imply that for simultaneous motions, there likely exist paths where a given arm segment can exploit the motion of its neighbors to reach its end position, therefore using less power. While the principle may be well understood for classical robotic systems, the contribution of CMGs to this effect is new and deserves additional attention.

V. Conclusions

This study demonstrates that CMGs are an effective actuation method for manipulating a payload in space. After deriving the equations of motion for an N-link CMG-driven system with a payload, we presented a PD control design for maneuvering the arm segments to desired joint angles. We demonstrated that for a single-body system, a mass-center offset affects only the inertial torque. However, since a two-body system exhibits coupled motions, the mass-center offset cannot be regarded as having an inertia-only effect unless the bodies are moved sequentially. We reasoned that when any one of the arm segments rotates while the others remain fixed, the resulting dynamics resemble the single-body case. Since this result may imply that sequential rotations reduce the system power consumption, we compared the cases in which bodies are moved simultaneously and sequentially for a large number of maneuvers. However, the mean energy expended is lower for simultaneous motions, suggesting that there exists an optimal steering path that minimizes the energy expended by the system. We leave this as a topic for future work. We hope that further analysis may provide a proof-of-concept for low-power space robotics. Although based on a simple idea, this technology has potential for in-orbit space-system construction and repair, both of which are of great interest in NASA's Vision for Space Exploration.

References

[1]Carpenter, M. D. and Peck, M. A., "Dynamics of a High-Agility, Low-Power Coelostat Telescope," *AIAA Guidance, Navigation, and Control Conference and Exhibit*, No. 2006-6591, Keystone, Colorado, Aug. 2006.

[2]Peck, M. A., Paluszek, M. A., Thomas, S. J., and Mueller, J. B., "Control-Moment Gyroscopes for Joint Actuation: A New Paradigm in Space Robotics," *AIAA 1st Space Exploraton Conference: Continuing the Voyage of Discovery*, Orlando, Florida, 2005.

[3]Peck, M. A., "Low-Power, High-Agility Space Robotics," *AIAA Guidance, Navigation, and Control Conference and Exhibit*, San Francisco, California, 2005.

[4]Crenshaw, J. W., "2-SPEED, A Single-Gimbal Control Moment Gyro Attitude Control System," *AIAA Guidance and Control Conference*, No. 73-895, Key Biscayne, Florida, Aug. 1973.

[5]Havill, J. R. and Ratcliff, J. W., "A Twin-Gyro Attitude Control System for Space Vehicles," Tech. Rep. NASA TN D-2419, Aug. 1964.

[6]Kane, T. R. and Levinson, D. A., *Dynamics: Theory and Applications*, McGraw-Hill, Inc., New York, 1985.

[7]Moon, F. C., *Applied Dynamics: With Applications to Multibody and Mechatronic Systems*, John Wiley and Sons, Inc., New York, 1998.

[8]Vukobratovic, M., *Introduction to Robotics*, Springer-Verlag, Berlin, Heidelberg, 1989.

[9]Hughes, P. C., *Spacecraft Attitude Dynamics*, Dover Publications, Inc., Mineola, New York, 1986.

[10]Honeywell, "Pointing and Momentum Control," http://www.honeywell.com/sites/aero/Pointing-Momentum-Control.htm, Accessed 8/2/07.

[11]Billing-Ross, J. A. and Wilson, J. F., "Pointing System Design for Low-Disturbance Performance," *AIAA Guidance, Navigation, and Control Conference*, Minneapolis, Minnesota, 1988, pp. 444–451.